

# **Performance of an RC Corner Beam-Column Joint Severely Damaged under Bidirectional Loading and Rehabilitated with FRP Composites**

**by M. Engindeniz, L.F. Kahn, and A.-H. Zureick**

**Synopsis:** This paper presents the performance of a full-scale reinforced concrete corner beam-column-slab specimen that was first severely damaged under bidirectional quasi-static loading, then rehabilitated and retested. The specimen was built using the pre-1970s construction practices including the use of low-strength materials (3000 psi [21 MPa], Grade 40 reinforcing bars) and deficiencies in reinforcement detailing. The rehabilitation process consisted of: (1) epoxy injection, (2) addition of a bar within the clear cover of the column at the inside corner, and (3) external application of a multilayer composite system made of unidirectional carbon-epoxy layers placed at different orientations. The carbon fiber-reinforced polymeric system was heat-cured at a temperature of  $80^{\circ}\pm10^{\circ}\text{C}$  ( $176^{\circ}\pm18^{\circ}\text{F}$ ) for 6 hours. The performance was evaluated both before and after rehabilitation based on the progression of damage and the hysteretic behavior including the changes in the strength, stiffness, and energy dissipation characteristics. The results indicated that even a severely damaged corner joint can be effectively rehabilitated using CFRP to achieve a ductile beam failure mechanism. The joint was upgraded to withstand story drift ratios of up to 3.7% applied simultaneously in both directions.

**Keywords:** beam-column joints; fiber-reinforced polymer; repair; strengthening

## 20 Engindeniz et al.

ACI member **Murat Engindeniz** is a PhD Candidate at the Georgia Institute of Technology, Atlanta, GA. He is an associate member of ACI Committee 440, Fiber Reinforced Polymer Reinforcement. His research interests include behavior of nonseismically designed reinforced concrete structures, seismic rehabilitation with high-performance materials, and large-scale testing.

**Lawrence F. Kahn**, FACI, is a Professor of civil engineering at the Georgia Institute of Technology, Atlanta, GA. He is Chair of ACI Committee 562, Evaluation, Repair, and Rehabilitation of Concrete Buildings, and a member of ACI Committees 364, Rehabilitation; 546, Repair of Concrete; Concrete Research Council; and TRRC.

**Abdul-Hamid Zureick** is a Professor of structural engineering, mechanics, and materials at the Georgia Institute of Technology, Atlanta, GA. His research interests include the design, testing, and construction of fiber-reinforced polymer composites for use in new construction and for the rehabilitation of existing structural systems.

### INTRODUCTION

Reinforced concrete (RC) buildings constructed with inadequate or no seismic considerations constitute a significant portion of the building stock in many countries. Many catastrophic failures during earthquakes have indicated the vulnerability of beam-column joints in such buildings. In the U.S., buildings constructed before the adoption of the first design guidelines for RC beam-column joints in 1976 (ACI 352R-76) typically have the following major deficiencies in the joint regions: (1) strong beams, weak columns, (2) little or no joint transverse reinforcement, (3) beam bottom reinforcements with short embedment length, (4) short lapped splices of column bars just above floor level, and (5) wide spacing of column ties (Beres et al. 1996).

The ACI-ASCE Committee 352 (ACI 352R-02) recommended that the adequacy of these joints be established and that methods of improving their performance be developed. A detailed review of the technical literature shows that such efforts, in general, have been limited to testing of one-way joint specimens with no floor slab or transverse beams (Engindeniz et al. 2005). As a result, most of the proposed strengthening schemes were not only geometrically inapplicable to actual frame joints, but they also did not account for force transfer mechanisms and damage modes created by the presence of floor members and bidirectional loading. In studies where such effects were considered, the improved performance of the strengthened specimens was shadowed by the labor-intensiveness and bulkiness of the proposed strengthening schemes (e.g. concrete jacketing).

Relative advantages and disadvantages of previously studied repair and strengthening techniques were presented elsewhere (Engindeniz et al. 2005). Among these techniques, externally bonded fiber-reinforced polymeric (FRP) composite applications offer advantages over others including ease of construction, corrosion resistance, and no increase in member sizes and mass. FRP composites are most attractive for their tailorability; the fiber-orientation in each ply can be adjusted so that specific strengthening objectives such as increasing the strength only, confinement only, or both, can be achieved (ACI 440.2R-02). Tests conducted to date on joint specimens with no floor members have shown that FRP composites can be promising for achieving ductile failure mechanisms if debonding of composites from the concrete surface can be delayed or prevented. Use of FRPs in rehabilitation of actual three-dimensional frame joints, however, requires testing with consideration of the presence of floor members and bidirectional loads. In addition, thermal properties such as the glass-transition temperature and rate of curing of the matrix systems used in rehabilitation should be assessed with respect to the operating temperatures that the rehabilitated structure is likely to face during its service life. Curing schedules so adjusted may also improve the bond between the composite systems and concrete (Ferrier 1999).

### RESEARCH SIGNIFICANCE

This research starts to answer “needed research” posed by ACI-ASCE Committee 352 “Design of Beam-Column Connections in Monolithic Reinforced Concrete Structures”, and it demonstrates the efficacy of CFRP for RC beam-column joint rehabilitation.

## EXPERIMENTAL PROGRAM

### Specimen Design

A full-scale corner beam-column-slab specimen was designed using the pre-1970s construction practices including deficient detailing and low-strength materials (specified  $f'_c=3000$  psi [21 MPa], Grade 40 reinforcing bars), and according to the ACI 318-63 code. From a review of the failure modes observed in previous studies in the literature, a column-to-beam moment strength ratio ( $\Sigma M_c/\Sigma M_b$ ) of approximately 0.9 was targeted in the design to ensure a failure mode involving damage to the joint. Such a design called for the overall dimensions and reinforcement details shown in [Figure 1](#). The major deficiencies expected to dominate the behavior of the specimen were: (1) actual  $\Sigma M_c/\Sigma M_b=0.86$ , (2) no joint shear reinforcements, (3) beam bottom bars with an embedment length of only 6 in. (150 mm) into the joint, (4) a short ( $20d_b$ ) and unconfined lapped splice of column longitudinal bars just above floor level.

### Material Properties

The specimen was cast in two lifts resulting in a cold joint at the bottom of the upper column. The average compressive strength of concrete ( $f'_c$ ) for the first lift was 2880 psi (19.8 MPa) on the 28th day and 3740 psi (25.8 MPa) on both test days (i.e. before and after rehabilitation). For the second lift,  $f'_c$  was 3600 psi (24.8 MPa) on the 28th day and 4950 psi (34.1 MPa) on the test days. The reinforcements consisted of #3, #5, and #6 Grade 40 deformed bars with average yield strengths of 54 ksi (372 MPa), 52 ksi (358 MPa), and 46 ksi (317 MPa), respectively.

### Test Setup

The specimen represents the part of the corner of a building isolated at the assumed inflection points (i.e. midspan of beams and columns) when the building is subjected to lateral loads. The test setup is shown in [Figure 2](#). The top of the column was connected to a universal joint that allowed rotation in any direction and vertical translation; only lateral translations were restrained. The bottom of the column was fixed to the strong floor; the length of the lower column was designed such that an inflection point would form below the beam at a distance equal to the length of the upper column. Cyclic lateral loads were simulated by hydraulic actuators mounted vertically at the end of the beams. In addition to the rotational releases at each end of the actuators about an axis perpendicular to the beams, a special fixture was used between the specimen and the actuators to permit torsional rotations expected due to the presence of the slab. The column axial load was applied using a fixture consisting of a DWYDAG rod running alongside each corner of the column and a hydraulic center-hole jack connected to each rod.

### Instrumentation of the As-Built Specimen

The strains in the reinforcing bars were monitored at the joint-beam, joint-column, and beam-slab interfaces in both EW and NS directions using electrical resistance strain gages mounted on the bars ([Figure 3a, b](#)). Strain gages were also mounted on two outer beam bottom bars in each direction at 3 in. (76 mm) into the joint, two stirrups above and below the joint (all four legs), and on a beam stirrup (two vertical legs) as shown in [Figure 3a](#). Joint shear strains and relative rotations of the beams and columns with respect to the joint were monitored using the LVDT configuration in [Figure 3c](#) on both S and W faces of the specimen. Additional measurement of the rotation of the beams with respect to the column was performed using string potentiometers mounted at the midwidth of the beam top and bottom surfaces ([Figure 3c](#)). Global rotations and translations of the joint region in both directions were measured with respect to a fixed reference frame using potentiometers ([Figure 3c](#)). Torsional rotations of each beam were monitored using potentiometers mounted on the inner and outer edges of the beam bottom surface at the tip of the beam and at a section near the column faces. The column shear forces were monitored by full-bridge strain gage configurations mounted on each arm of the triangular reaction frame connected to the universal joint atop the column. The column axial load was monitored by a load cell mounted on each hydraulic jack at each corner of the column.

### Loading Procedure

The loading procedure simulated a cyclic lateral loading of a building carrying service gravity loads. First, a column axial load of 10% of the column's compressive load capacity was gradually applied ( $0.1P_o=74$  kip [330 kN]). Then, both beams were deflected downwards in a displacement-controlled mode until the strong-axis beam moments at the column faces were brought to a level that was estimated to occur in an actual frame building under service loads. The beams were then subjected to cyclic loading symmetrically around this deformed position in a displacement-controlled mode as shown in [Figure 4](#).

The applied displacement history included unidirectional cyclic loading of EW and NS beams, respectively, at a displacement level of  $\pm\Delta_y$ , which was followed by bidirectional simultaneous cyclic loading of both beams at displacement levels  $\pm\Delta_y$ ,  $\pm 1.5\Delta_y$ ,  $\pm 2.0\Delta_y$ , and  $\pm 4.0\Delta_y$ . The objective of the unidirectional loading was to compare the behavior of the specimen to that under biaxial loading in the later cycles. The displacement at first yield,  $\Delta_y$ , was determined by continuously monitoring the strains in all column and beam critical sections during the first stage of loading. The first yield occurred in the upper column at the inside (NE) corner at a displacement of  $\pm\Delta_y=1.12$  in. (28.5 mm) measured from the reference deformed position used for cyclic loading. As a result, the applied displacement levels corresponded to interstory drift ratios ( $\theta$ ) of  $\pm 0.93\%$ ,  $\pm 1.40\%$ ,  $\pm 1.87\%$ , and  $\pm 3.73\%$ . Three cycles were applied at each unidirectional or bidirectional drift level to determine cyclic degradation. A displacement rate of 0.2 in./min (5.1 mm/min) was used until the beginning of the  $\pm 1.87\%$  drift cycles, at which point the rate was increased to 0.3 in./min (7.6 mm/min). The loading of the as-built specimen was terminated after the  $\pm 1.87\%$  drift cycles upon achieving a severe level of damage, thus preventing the specimen to become unstable under the applied loading condition. After rehabilitation, the specimen was subjected to the entire displacement history.

The following terminology is used throughout this paper: Positive direction for actuator displacements are upwards. A load step consists of moving to a certain drift level in one direction, then moving back to the reference position. A load cycle consists of a load step in the negative direction followed by another in the positive direction. A drift level that is applied simultaneously in the EW and NS directions is referred to as a bidirectional drift.

## PERFORMANCE OF THE AS-BUILT SPECIMEN

### Overall Behavior

The behavior of the as-built specimen was dominated by a combination of four major damage modes:

1. Yielding in the upper column during the negative load steps. The first peak at -0.93% drift in the EW direction represents the first yield accompanied by wide flexural cracks at the inside (NE) corner of the upper column. The demand at this corner increased significantly during the bidirectional cycles, the width of the cracks reaching 0.1 in. (2.5 mm) and 0.25 in. (6.4 mm) at the first peaks at -1.40% and -1.87% drift, respectively. The first yield in the lower column also occurred at the first peak at -1.87% drift.
2. Slippage/pull-out of beam bottom bars during the positive load steps. Flexural cracks at the beam-column interfaces extending vertically from the bottom to the middepth of the beams reached a maximum width of 0.06 in. (1.5 mm) during the unidirectional cycles and 0.08 in. (2.0 mm), 0.2 in. (5.1 mm), and 0.31 in. (7.9 mm) at the +0.93%, +1.40%, and +1.87% bidirectional drift levels, respectively. The strain readings indicated that the bottom bars near the inside faces of the beams were subjected to larger tensile forces than those on the outside. Although the bars performed well during the unidirectional cycles, and the inner bars developed strains as high as  $1360 \mu\epsilon$  ( $\varepsilon_y=1660 \mu\epsilon$ ), they lost their anchorage gradually after the beginning of the bidirectional cycles. A comparison of strains just outside the joint with those at 3 in. (76 mm) into the joint indicated that, by the end of test, only the bars on the outside were left with a limited anchorage.
3. Joint shear cracking during the negative load steps. [Figure 5](#) shows that diagonal cracking in the joint occurred in one direction only and not in the often recorded "X" manner, because the loss of anchorage of the beam bottom bars prevented the formation of the other diagonal crack. The maximum width of the joint shear cracks was 0.04 in. (1.0 mm) during the unidirectional cycles. During the bidirectional cycles, they not only opened wider in the plane of the joint panel, but they also exhibited bulging in the direction perpendicular to the surface due to rotation of the hooked beam top bars. At the second peak at -0.93% bidirectional drift, these cracks had joined those at the bottom of the beam and reached a width of 0.07 in. (1.8 mm) to 0.08 in. (2.0 mm).

4. Propagation of cracks into the upper column. At the first peak at -1.40% drift, the diagonal crack in the joint panel propagated vertically into the upper column forming a combined crack extending from the bottom of the beam into the upper column, exhibiting a bulging of up to 0.25 in. (6.4 mm) in the later cycles. At the end of the test, this crack measured 0.31 in. (7.9 mm) wide at the beam embedment region, 0.25 in. (6.4 mm) wide in the joint panel, and 0.125 in. (3.2 mm) in the upper column ([Figure 5a, b](#)). The cracks in EW and NS faces were connected through the joint at an angle of roughly 45 degrees, forming a large triangular prismlike concrete block trying to separate from the outside corner of the column. The two stirrups along the column lapped splice resisted this separation by developing strains as high as 1550  $\mu\epsilon$  in their S and W legs.

The maximum tensile strains achieved in the beam top bars provide a means of comparing the specimen's performance with a desirable ductile beam hinging mechanism. The strain measurements at the NS beam-column interface showed that while the outermost top bar developed 90% of its yield strain during the bidirectional cycles, the innermost top bar developed only 42%. A similar strain distribution was recorded at the EW beam-column interface. Such a strain distribution is attributed to combined unsymmetric bending and torsion in the beams due to the presence of the slab. The measured strain levels indicated that a significant strengthening of the column and the joint was needed to achieve yielding in all beam top bars.

Two major cracks were observed in the slab:

1. A flexural crack that formed in a direction parallel to the NS beam at 3.5 in. (89 mm) from the inside face of this beam and propagated across the entire width and through the thickness of the slab—This crack initiated during the EW unidirectional cycles and reached a maximum width of 0.02 in. (0.5 mm). Such a crack did not occur in the EW direction during the NS unidirectional cycles.
2. A diagonal crack at the bottom surface extending from the joint region to the opposite corner—This crack was located after completing the test and measured 0.04 in. (1.0 mm)-wide. It indicated the need for special diagonal reinforcement in the slab corners in line with the requirements of ACI 318-05, Section 13.3.6.

### Hysteretic Behavior

The strength, stiffness, and energy dissipation characteristics of the specimen were evaluated through the force-drift hysteretic response, presented in [Figure 6](#) for both EW and NS directions. The curves are shifted from the horizontal line representing zero load due to the initial loads on the actuators (EW=2.0 kip [8.9 kN], NS=2.7 kip [12.0 kN]) at the deformed position used as the reference level for cyclic loading. This deformed position is the "zero" drift datum. Positive load values indicate compression force in the hydraulic ram.

The peak loads measured in each cycle in both negative and positive loading directions are presented in [Table 1](#). The maximum loads in both positive and negative directions occurred in the first unidirectional cycles. A significant decrease in the peak loads was observed at the beginning of the bidirectional cycles, then the strength degraded more gradually. Both the overall and cyclic strength degradation were more pronounced in the negative direction as a result of the progressive damage in the joint panel and in the upper column.

Significant degradation in stiffness and pinching of the curves were dominant throughout the hysteresis loops. The peak-to-peak stiffness  $K_p$ , defined as the slope of the line connecting the peak of a negative load step to that of the next positive load step, decreased continuously as shown in [Figure 7](#). An 80% decrease in  $K_p$  from the first cycle to the last cycle was observed in the EW direction; the decrease in  $K_p$  in the NS direction was 78%. The degradation in stiffness was more significant after the beginning of the bidirectional cycles.

The energy dissipated by the specimen was calculated as the area enclosed by the force-displacement curves. Cumulative plots of the dissipated energy in both EW and NS directions are presented in [Figure 8](#). Although the total energy increased continuously, the increase was not proportional to the increase in the applied displacements due to the combined effects of increased pinching and strength degradation.

The plot of the joint shear stress factor ( $\gamma$ ) versus the joint shear strain ( $\gamma_s$ ) is presented in [Figure 9](#), where  $\gamma = V_{jh} / \sqrt{f'_c b_j h_c}$  as defined in ACI 352R-02, Sec. 4.3.1. The horizontal joint shear force ( $V_{jh}$ ) was determined as the difference between the column shear force and the total tensile normal force ( $T$ ) acting on the beam-joint interface.  $T$  was estimated by assuming a constant moment-arm of  $jd=0.875d$  between the tension and compression resultants at this section (i.e.  $T=M/0.875d$ ).  $\gamma_s$  for each joint panel was taken as the average of four joint shear strain estimates obtained from the LVDT configuration in [Figure 3c](#). The resulting  $\gamma$  versus  $\gamma_s$  plots were in line with all

previous discussions in that significant softening and distortion of the joint during the negative load steps was clear. Maximum shear stresses were in the negative direction, the  $\gamma$  factor being  $5.7 \sqrt{\text{psi}}$  ( $0.47 \sqrt{\text{MPa}}$ ) and  $4.9 \sqrt{\text{psi}}$  ( $0.41 \sqrt{\text{MPa}}$ ) for the EW and NS directions, respectively. For the positive loading direction, maximum  $\gamma$  values of  $4.2 \sqrt{\text{psi}}$  ( $0.35 \sqrt{\text{MPa}}$ ) and  $4.5 \sqrt{\text{psi}}$  ( $0.37 \sqrt{\text{MPa}}$ ) were obtained for the EW and NS directions.

The shear capacity of the joint may be underestimated by the use of the “constant moment-arm approximation” because of the unaccounted contributions to the tensile forces in the beam bars. Data not included here for brevity suggests that torsion, for instance, increases the tensile forces in all the beam bars. Even so, this method can be used to compare the joint shear strength before and after rehabilitation.

## REHABILITATION PROCEDURE

All rehabilitation steps were performed at the deformed position used as reference for cyclic loading. The specimen was first repaired by pressure-injection of a high-strength, high-modulus, low-viscosity epoxy that filled all cracks larger than 0.01 in. (0.3 mm) [Figure 10a]. The injection of approximately 2 gal. (7.6 L) of epoxy confirmed the severity of damage in the specimen.

### Strengthening Design and Application

The specimen was strengthened to achieve improvements in the following areas: (1) flexural strength of the column, (2) joint shear strength, (3) beam bottom bar anchorage, (4) column end confinement, and (5) flexural strength at the SW corner of the slab. Strengthening in all areas except (1) was performed using a 9 oz/yd<sup>2</sup> (300 g/m<sup>2</sup>) unidirectional carbon fabric impregnated with a high-strength, high-modulus epoxy matrix using a hand-layup technique. During the preliminary design of the experiment, tensile properties of the carbon-epoxy system were taken as those reported by the manufacturer (i.e. tensile strength  $P_u^{\text{CFRP}}=2100 \text{ lb/in./layer}$  [370 N/mm/layer], ultimate strain  $\epsilon_u^{\text{CFRP}}=1.00\%$ , thickness  $t=0.020 \text{ in./layer}$  [0.5 mm/layer]). The properties attained in the actual application were examined by testing coupons cut from a single-layer plate (i.e. witness plate) made using the same technique and curing schedule (see next section) as that used in rehabilitating the specimen. The witness plate contained 42% fibers by weight, which corresponded to a fiber volume ratio of approximately 34% assuming a 4% void volume in the system. Based on 10 coupon tests, the following average values were obtained:  $P_u^{\text{CFRP}}=2930 \text{ lb/in./layer}$  (510 N/mm/layer),  $\epsilon_u^{\text{CFRP}}=1.52\%$ , and  $t=0.027 \text{ in./layer}$  (0.7 mm/layer).

The following approach was taken in the design and application of strengthening in each area:

1. **Flexural strength of the column.** The higher force demand on the inside corner of the upper column required addition of flexural reinforcement along the entire height of the column and continuous through the slab. The amount of existing column longitudinal reinforcement (2#5) at this corner was doubled by removing a 2 in. x 2 in. (50 mm x 50 mm) portion of the column corner including a perforation in the slab, adding a #7 bar ( $f_y=65 \text{ ksi}$  [448 MPa]) (Figure 10c), and recasting the corner with a polymer-modified, cementitious mortar ( $f'_c=7200 \text{ psi}$  [49.6 MPa] on the test day).
2. **Joint shear strength.** The maximum horizontal joint shear force ( $V_{jh}^{\max}$ ) that could develop was estimated by assuming yielding of all beam top bars and the three slab bars within 20 in. (510 mm) (ACI 318-05, Sec. 8.10.3) next to the beams:

$$V_{jh}^{\max} = \sum A_s f_y - V_{col} = 6(A_s f_y)_{\#6} + 3(A_s f_y)_{\#3} - \frac{M_n^-}{L_b} 1.25 \quad (1)$$

where  $M_n^-$  is the negative moment capacity of the beam,  $L_b$  is the beam length measured from column face, and 1.25 is the ratio of the beam end load to column shear ( $V_{col}$ ) analytically determined for this test setup using the measured material properties. Three layers of CFRP oriented perpendicular to the longitudinal axis of the column (90 degrees) were required to resist this force according to Equation 2:

$$n_{jh} = \frac{V_{jh}^{\max}}{h_j P_u^{\text{CFRP}}} \quad (2)$$

where  $n_{jh}$  is the number of layers,  $h_j$  is the height of the joint covered with CFRP (20 in. [510 mm]), and  $P_u^{\text{CFRP}}$  is the average tensile strength (lb/in./layer) of CFRP ( $n_{jh}=2.62=3$ ). An additional two layers oriented at 0 degree (parallel to the column) were provided to resist the vertical component of the principal tension force in

the joint panel. All layers were extended into the upper and lower columns by a distance equal to the height of the confined regions at the column ends. All five layers were applied on the S and W faces of the specimen only.

3. **Beam bottom bar anchorage.** Although the demand was larger on the bottom bars near the inside faces of the beams than on those near the outside faces, for ease of construction, an attempt was made to improve the positive moment capacity of the beams by providing CFRP reinforcement on the outside faces only. CFRP strips were placed around the SW corner of the joint such that the strips extended 28 in. (710 mm) on to the beams measured from the beam-column interfaces (“Area 4” in [Figure 10g](#)). The number of layers ( $n_{strip}$ ) was selected such that the load capacity of the strips would be equivalent to that of all three bottom bars at yield:

$$n_{strip} = \frac{\sum A_s f_y}{w_s P_u^{CFRP}} = \frac{3(A_s f_y)_{\#6}}{w_s P_u^{CFRP}} \quad (3)$$

The width of the strips ( $w_s$ ), preferred to be less than half the beam depth to avoid an undesirable increase in the negative moment capacity of the beams, was arbitrarily selected as 7 in. (180 mm); this resulted in  $n_{strip} = 4.13 = 5$ . An anchorage length of 28 in. (710 mm) was selected so that the distance from the tip of the beam bottom bars to the end of the strips would be equivalent to the development length of these bars according to ACI 318-05, Sec.12.15.

4. **Column end confinement.** The CFRP used for confinement of the column ends was designed per ACI 440.2R-02, Sec. 11.3 such that the effective usable compressive strain in concrete would be equivalent to that provided by the hoop reinforcement required by ACI 318-05, Sec. 21.4.4. This approach called for two layers (90 degrees) of wrapping at the column ends over a length of 18 in. (460 mm) [“Area 1” in [Figure 10g](#)]. Wrapping the column ends also provides an effective means of anchorage for the layers extended from the joint onto the columns as well as for the column longitudinal bar added in the NE corner.
5. **SW corner of the slab.** A 48 in. x 48 in. (1220 mm x 1220 mm) triangular portion of the bottom surface was strengthened with two layers of CFRP to increase the flexural strength to an extent required by ACI 318-05, Sec. 13.3.6. The fibers in both layers were oriented in the NW-SE direction (“Area 5” in [Figure 10h](#)). Strengthening at the top surface was deemed unnecessary due to limited cracking in this region.

It is to be noted that the use of the manufacturer’s reported nominal CFRP properties in the design and rounding up of the resulting numbers of required layers (e.g.  $n_{jh}$ ,  $n_{strip}$ ) to whole numbers lead to the use of a few more layers of CFRP than what would be used if the properties attained in the actual application were known. For instance, the as-attained properties would lead to  $n_{jh}=2$  (instead of 3) and  $n_{strip}=3$  (instead of 5); the efficacy of such a configuration is to be studied in subsequent experiments.

### Curing of CFRP

Our differential scanning calorimetry (DSC) tests conducted on the matrix system used for the FRP system showed that room temperature-cured Sikadur 330 US epoxy had glass transition temperature ( $T_g$ ) values of 49°C (122°F) and 56°C (133°F) after 9 and 60 days, respectively. This raised a concern about the mobility of the epoxy molecular chain structure in an operating temperature range that is often encountered in the vast majority of regions around the world. It is often recommended that the FRP system have a  $T_g$  of 10°C (18°F) to 30°C (54°F) higher than the operating temperature (e.g. Zureick and Kahn 2001; MIL-17 2002; AFGC 2003).

To achieve an acceptable degree of molecular cross-linking, the matrix system was heat-cured at 80°C (176°F) for a duration of 3 hours or more. DSC results indicated that, after 3 hours, the  $T_g$  was increased to 70°C (158°F). Subsequently, all areas of the specimen that were strengthened with CFRP were heat-cured at a temperature of  $80 \pm 10^\circ\text{C}$  (176  $\pm$  18°F) for 6 hours instead of 3 hours, an arbitrary decision that was based on the fact that part of the heat would be absorbed by concrete. Heat-curing was performed by building a sealed, insulated wooden box around the region, and then heating the enclosed region with four adjustable heat guns ([Figure 10f](#)). DSC tests conducted on samples taken from the FRP system after the completion of the test program resulted in  $T_g$  values between 63°C (145°F) and 65°C (149°F).

### Layup Sequence

The CFRP layers were stacked in a sequence that would result in a symmetric layup in all areas. A symmetric layup was necessary to: (1) prevent curvatures during heat-curing that could cause early debonding from the

concrete surface, and (2) eliminate the extension-bending coupling that would result in difficulties associated with the determination of the tensile properties of the FRP system. The final stacking sequences in all areas are shown in Figure 10g, h.

#### Instrumentation of the Rehabilitation Components

The strains in the added #7 bar at sections above and below the beams were monitored using two strain gages at each section (Figure 3e). The strains in the FRP strips bonded on each beam were monitored using three strain gages mounted on the strips at a section 4 in. (102 mm) away from the beam-joint interface (Figure 3d). These gages were evenly spaced with the bottom one being at the level of the beam bottom bars. Strain gages were also mounted on the column end wraps at the midwidth of the column at the first and second stirrup levels above the joint and at the third stirrup level below the joint (Figure 3d).

### **PERFORMANCE AFTER REHABILITATION**

#### Overall Behavior

After rehabilitation, the poor behavior of the as-built specimen was improved to a desirable strong column-weak beam behavior. The initiation of damage was delayed until the beginning of the bidirectional cycles, and the damage modes leading to the failure of the specimen started to occur only after the  $\pm 1.87\%$  drift cycles. Improvements in performance are summarized below in reference to the damage modes that dominated the behavior of the specimen before rehabilitation:

1. **Onset and progression of bar yielding.** The first yield was delayed until the first peak at -0.93% bidirectional drift at which point yielding occurred in both beams and in the slab. The second beam top bars from outside in both beams and a slab top bar parallel to the NS near the column yielded, the outermost beam top bars just reached their yield strain ( $\varepsilon_y=1660 \mu\epsilon$ ), and the strains in the other beam top bars ranged from 1230  $\mu\epsilon$  to 1330  $\mu\epsilon$ . The flexural cracks near the top of both beams measured 0.02 in. (0.5 mm) wide. At the first peak at -1.40% drift, the two outer beam top bars in each beam and two slab top bars near the column parallel to each beam had yielded; the other beam top bars had just reached their yield strain. The flexural cracks near the top of the beams measured 0.07 in. (1.8 mm) and 0.05 in. (1.3 mm) wide for the EW and NS beams. The #7 bar added in the NE corner of the column reached its yield strain ( $\varepsilon_y=2490 \mu\epsilon$ ) in the upper column at the first peak at -1.87% drift at which point all beam top bars except for the innermost NS beam top bar had yielded, and the cracks in the EW and NS beams were 0.15 in. (3.8 mm) and 0.08 in. (2.0 mm) wide. During the  $\pm 1.87\%$  and  $\pm 3.73\%$  drift cycles, the EW beam underwent more damage than the NS beam, and the strains in the beam bars increased more rapidly than in the column bars as drift increased. At the first peak at -3.73% drift, the EW beam underwent severe spalling. The innermost NS beam top bar did not yield throughout the test but developed strains as high as 1490  $\mu\epsilon$ . While the NS beam top bars that did yield developed strains as high as 14,080  $\mu\epsilon$ , the demand on the column was limited to a maximum strain of 5250  $\mu\epsilon$  in the added #7 bar in the upper column and spalling of the inside corner of the joint near the first negative peak at -3.73% drift.
2. **Beam bottom bar anchorage.** The FRP strips bonded on the beams ("4" in Figure 10g) prevented the distress from concentrating at the column face. At the third peak at +0.93% bidirectional drift, distress consisted of 0.01 in. (0.3 mm)-wide flexural cracks at the bottom surfaces of the beams distributed over a distance of 50 in. (1270 mm) from the column face, and cracks at the beam-column interface measuring 0.01 in. (0.3 mm)-wide under the FRP strips and 0.04 in. (1.0 mm)-wide near the inside corner of the column. At the first peak at +1.40% drift, a complete debonding of the FRP strips on the NS beam took place suddenly, initiating at the beam-column interface and moving along the beam. The FRP strips developed a maximum strain of 4570  $\mu\epsilon$  at the level of the beam bottom bars. The strips on the EW beam were debonded over a distance of 10 in. (250 mm) from the beam-column interface, and complete debonding did not occur until the first peak at +1.87% drift. A maximum strain of 3920  $\mu\epsilon$  was developed in these EW strips. After debonding of the FRP strips, the beams lost much of their improved behavior in positive bending. A thin layer of concrete attached to the debonded strips indicated the need for better anchorage schemes for these strips so the resulting interfacial and normal stresses can be maintained by the concrete.
3. **Joint shear capacity.** The problem of joint shear failures prior to ductile failure of the beams was resolved. Although very small portions of the FRP system in the joint ("2" and "3" in Figure 10g) started to debond near

the beam-joint interfaces during the  $\pm 1.87\%$  drift cycles, the failure of the joint required a drift of  $-3.73\%$ , at which point the beams had undergone significant yielding and damage. The failure of the joint involved crushing of the joint core and separation of the FRP system with large pieces of the joint concrete attached to it. This indicated a remarkable performance of the FRP system in maintaining the bond to concrete until the failure of the joint concrete.

4. **Column end confinement.** No significant signs of damage were observed at the column ends throughout the test. The tendency of the upper column to expand just above the joint was prevented by the FRP wrap which developed strains as high as  $9730 \mu\epsilon$  and  $6880 \mu\epsilon$  at the first stirrup level in the W and S faces, respectively, at the third peak at  $-3.73\%$  drift. At this point, the W leg of the first stirrup above the joint had just yielded ( $\epsilon_y=1960 \mu\epsilon$ ), and the other legs had developed strains up to  $1720 \mu\epsilon$ . The strains measured at the second stirrup level 11.5 in. (290 mm) above the slab indicated that there was no tendency of the column to expand.

The epoxy-injected cracks in the slab did not reopen but new cracks formed next to them and at other locations. At the bottom surface, a diagonal crack with a maximum width of 0.05 in. (1.3 mm) formed between the edge of the triangular FRP-strengthened region and the outer corner, which was accompanied by two other cracks extending from the corners of the triangular region in a direction parallel to the diagonal. At the top surface, flexural cracks formed near both EW and NS beam-slab interfaces across the entire width of the slab (width  $\leq 0.03$  in. [0.8 mm]). Additional flexural cracks formed in both directions away from the beams with widths up to 0.02 in. (0.5 mm).

### Hysteretic Behavior

The hysteretic behavior of the specimen before and after rehabilitation are compared in [Figure 6](#) through [Figure 9](#) and in [Table 1](#).

The strong column-weak beam behavior manifested itself in the force-drift hysteresis loops ([Figure 6](#)) as increases in the negative peak loads that were maintained until the first peak at  $-3.73\%$  drift, after which deflection the peak loads decreased due to significant damage in the beams. The maximum negative loads were increased by 57% and 70% for the EW and NS beams, respectively, when compared with those obtained for the as-built specimen. For the positive loading direction, up to 40% and 27% increases in the maximum loads were achieved for the EW and NS beams, respectively, until the FRP strips on the side of the beams debonded. Debonding of the strips are marked "7b" and "10b" on the hysteretic plots in [Figure 6](#). Percent increases in the peak loads were calculated with respect to the initial loads on the actuators at the deformed position used as reference for cyclic loading, represented by horizontal dashed lines in [Figure 6](#).

The increases in peak-to-peak stiffness ( $K_p$ ) during the bidirectional cycles ranged from 82 to 160% for the EW direction and from 68 to 117% for the NS direction ([Figure 7](#)). Unlike in the as-built specimen, much of the initial stiffness was maintained through the bidirectional cycles especially until debonding of the FRP strips on the beams.

The increase in the amount of energy dissipated by the specimen after the onset of yielding in the beams is clearly observed in [Figure 8](#). Until the end of the  $\pm 1.87\%$  drift cycles, where loading of the as-built specimen was terminated, the rehabilitated specimen dissipated 39% and 37% more energy in the EW and NS directions, respectively. During the  $\pm 3.73\%$  drift cycles, the amount of the dissipated energy was doubled; a majority of this energy was dissipated during the first cycle where a complete ductile failure of the beams was achieved.

The shear stress-strain behavior of the joint was improved significantly toward a desirable "rigid joint" behavior ([Figure 9](#)). Notable distortion of the joint occurred only after crushing of the joint concrete at the first peak at  $-3.73\%$  drift. The maximum joint shear stress factors ( $\gamma$ ) of  $8.3 \sqrt{\text{psi}}$  ( $0.69 \sqrt{\text{MPa}}$ ) and  $8.0 \sqrt{\text{psi}}$  ( $0.66 \sqrt{\text{MPa}}$ ) obtained for the negative loading direction for the EW and NS directions represent increases of 46% and 63% over the values obtained for the as-built specimen. As previously discussed, the actual shear strength of the joint may be underestimated by the "constant moment-arm approximation" used in determining the reinforcing bar tensile forces at the beam-joint interfaces. For example, another estimate of  $\gamma$  can be obtained for the load state where all the EW beam top bars and two slab top bars near this beam have yielded. Assuming that the second layer of beam top reinforcements have also yielded (not instrumented), and not considering any strain hardening, a  $\gamma$  value of approximately  $10.8 \sqrt{\text{psi}}$  ( $0.90 \sqrt{\text{MPa}}$ ) was obtained. Such a  $\gamma$  value is very close to that recommended by the ACI 352R-02 for use in the design of new corner joints that have members required to dissipate energy through reversals of deformation into the inelastic range (i.e. Type 2 joints:  $\gamma=12 \sqrt{\text{psi}}$  [ $1.00 \sqrt{\text{MPa}}$ ]).

## CONCLUSIONS

The following conclusions were drawn from the experimental results presented in this paper:

1. The behavior of a nonseismically designed reinforced concrete corner beam-column joint was dominated by a combination of column bar yielding, joint shear failure, and loss of anchorage of beam bottom bars.
2. Consideration of bidirectional loading and presence of all floor members revealed damage modes that may be overlooked in two-dimensional tests and analyses (e.g. larger demands on the inside corner of the column and on the beam bottom bars near the inside faces of the beams).
3. Even a severely damaged corner joint was efficiently rehabilitated to meet the strong column-weak beam criterion through easy-to-implement procedures such as the addition of a reinforcing bar within the clear cover of the column and the bonding of a CFRP system that was heat-cured in place.
4. Development of the positive moment capacity of the beam needs improvement. CFRP strips bonded on the outside faces of the beams were effective in anchoring the beam bottom bars, and they developed the yield stress in the exterior bar in the EW beam. But the full ductile capacities of the exterior bars were not developed, and the interior bottom bars were not brought to yield. Improvement in the anchorage of these CFRP strips and/or additional strengthening near the interior beam bottom bars may be needed.
5. Heat-curing of the composite system in place provided an effective means for achieving a full cure of the epoxy matrix quickly and for increasing the glass-transition temperature to values above the maximum operating temperature. While a superior composite-concrete bond was also achieved for the current specimen, additional data are necessary to evaluate the contribution of heat-curing to this performance.

The scope of this paper was limited to discussion of the global behavior of the specimen. A more detailed investigation of the internal force transfer mechanisms that lead to this global behavior will be the subject of a future publication.

## ACKNOWLEDGMENTS

This work was funded by the School of Civil and Environmental Engineering at the Georgia Institute of Technology. Sika Corp. donated Sikadur® 35 Hi-Mod LV LPL epoxy, SikaWrap® Hex 117C carbon fabric, Sikadur® 330 US epoxy, and SikaTop® 111 Plus mortar; LaFarge donated all ready-mix concrete; Gerdau Ameristeel Corp. fabricated the reinforcing bars; and Engineered Restorations, Inc. epoxy-injected the specimen. Their donations are gratefully acknowledged. The authors would also like to thank the Georgia Chapter of the International Concrete Repair Institute and its members for their comments and suggestions.

## REFERENCES

- ACI Committee 318 (1963), "Building Code Requirements for Reinforced Concrete (ACI 318-63)," American Concrete Institute, Detroit, MI, 144 pp.
- ACI Committee 318 (2005), "Building Code Requirements for Structural Concrete (ACI 318-05) and Commentary (318R-05)," American Concrete Institute, Farmington Hills, MI, 430 pp.
- ACI-ASCE Committee 352 (1976), "Recommendations for Design of Beam-Column Joints in Monolithic Reinforced Concrete Structures (ACI 352R-76)," ACI Journal, Proceedings V. 73, No. 7, pp. 375-393.
- ACI-ASCE Committee 352 (2002), "Recommendations for Design of Beam-Column Connections in Monolithic Reinforced Concrete Structures (ACI 352R-02)," American Concrete Institute, Farmington Hills, MI, 37 pp.
- ACI Committee 440 (2002), "Guide for the Design and Construction of Externally Bonded FRP Systems for Strengthening Concrete Structures (ACI 440.2R-02)," American Concrete Institute, Farmington Hills, MI, 45 pp.
- AFGC (2003), "Réparation et Renforcement des Structures en Béton au Moyen des Matériaux Composites – Recommandations Provisoires," Association Française de Génie Civil, 148 pp.
- Beres, A.; Pessiki, S. P.; White, R. N.; and Gergely, P. (1996), "Implications of Experiments on the Seismic Behavior of Gravity Load Designed RC Beam-to-Column Connections," *Earthquake Spectra*, V. 12, No. 2, pp. 185-198.

Engindeniz, M.; Kahn, L. F.; and Zureick, A. (2005), "Repair and Strengthening of Reinforced Concrete Beam-Column Joints: State of the Art," *ACI Structural Journal*, V. 102, No. 2, pp. 187-197.

Ferrier, E. (1999), "Comportement de l'Interface Composite-Beton sous des Sollicitations de Fluage Thermo-Stimulé et en Fatigue Oligocyclique. Application au Calcul Prévisionnel de la Durabilité de Poutres ba Renforcées," *Ph.D. Thesis*, L'Université Claude Bernard Lyon 1, Lyon, France, 263 pp.

*The Composite Materials Handbook-MIL 17* (2002), "Guidelines for Characterization of Structural Materials," V. 1, Published jointly by Technomic Publishing Co., Inc, and Materials Sciences Corporation in cooperation with ASTM, Lancaster, PA 17604, USA.

Zureick, A., and Kahn, L. (2001), "Rehabilitation of Reinforced Concrete Structures Using Fiber-Reinforced Polymer Composites," *ASM Handbook*, ASM International, V. 21, pp. 906-913.

Table 1 — Peak Loads

			EW		NS				
		Before Rehab		After Rehab		Before Rehab		After Rehab	
Drift, $\theta$	Cycle	$-P_{max}$ (kip)	$+P_{max}$ (kip)	$-P_{max}$ (kip)	$+P_{max}$ (kip)	$-P_{max}$ (kip)	$+P_{max}$ (kip)	$-P_{max}$ (kip)	$+P_{max}$ (kip)
EW $\pm 0.93\%$	1	-5.83	10.64	-9.11	13.73	*		*	
	2	-4.97	10.28	-8.68	13.42	*		*	
	3	-4.62	9.98	-8.43	13.22				
NS $\pm 0.93\%$	1					-4.03	11.40	-7.13	13.75
	2	*		*		-3.74	10.91	-7.20	13.33
	3					-3.46	10.64	-6.98	13.08
Biaxial $\pm 0.93\%$	1	-2.35	8.79	-7.25	12.93	-1.84	9.40	-6.24	12.56
	2	-1.75	8.51	-6.89	12.54	-1.21	9.04	-5.87	12.20
	3	-1.35	8.29	-6.63	12.39	-0.85	8.80	-5.60	12.03
Biaxial $\pm 1.40\%$	1	-2.46	8.31	-10.23	14.08	-1.91	9.02	-8.77	10.88
	2	-1.13	7.72	-8.86	13.39	-0.97	8.44	-7.65	10.20
	3	-0.61	7.45	-8.00	12.99	-0.42	8.14	-6.84	9.85
Biaxial $\pm 1.87\%$	1	-1.45	7.86	-9.86	11.11	-1.06	8.53	-8.15	10.23
	2	-0.10	7.52	-7.97	10.35	-0.02	8.01	-6.55	9.75
	3	0.28	7.30	-6.99	9.92	0.66	7.71	-5.55	9.46
Biaxial $\pm 3.73\%$	1			-9.63	9.43			-6.83	10.41
	2	**		-4.88	8.58	**		-2.71	9.32
	3			-2.31	8.21			-1.08	***

\* Peak loads during the unidirectional cycles are reported for the direction of loading only.

\*\* Testing of the as-built specimen was terminated after the  $\pm 1.87\%$  bidirectional drift cycles.

\*\*\*  $+P_{max}$  in this cycle could not be recorded due to a data acquisition problem.

1 kip = 4.448 kN

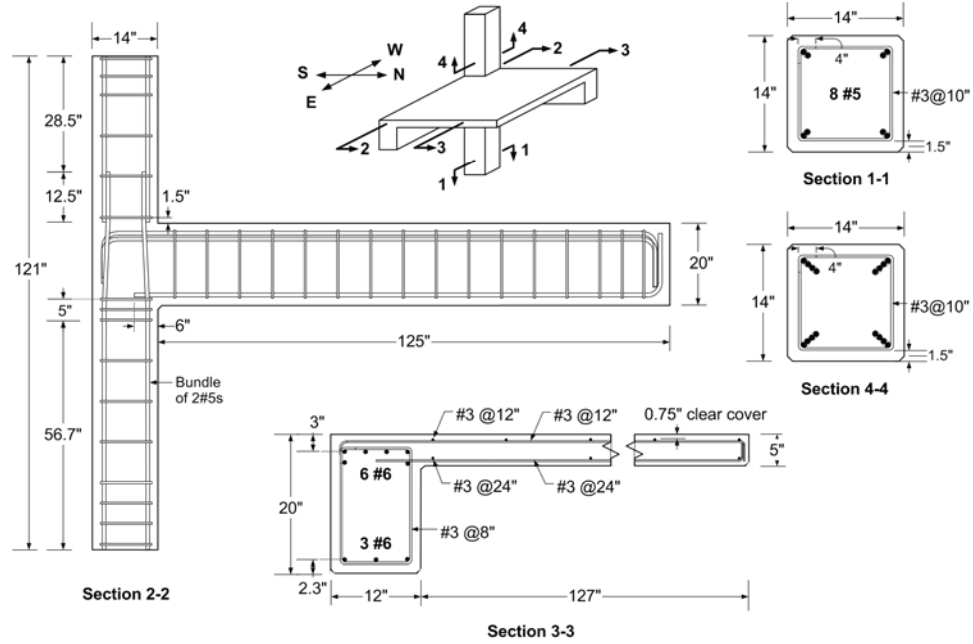


Figure 1 — Reinforcement details (1 in. = 25.4 mm).

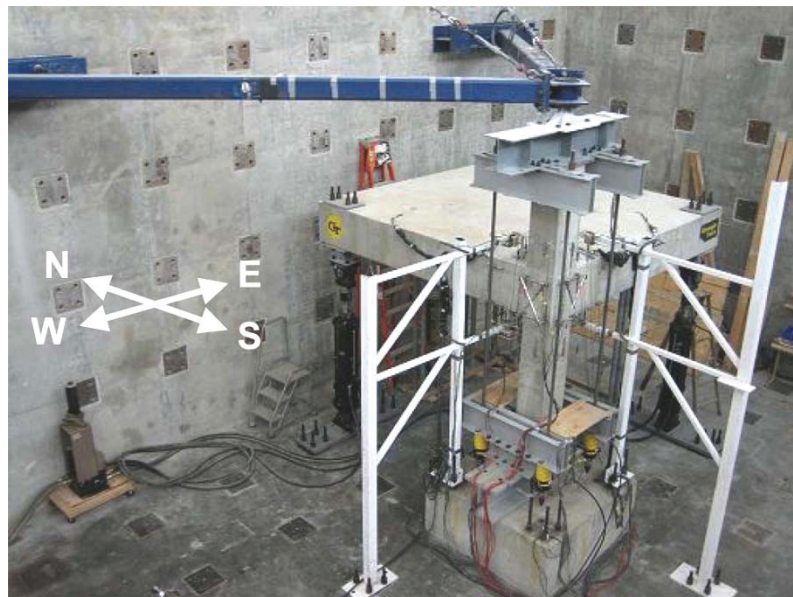


Figure 2 — Test setup.

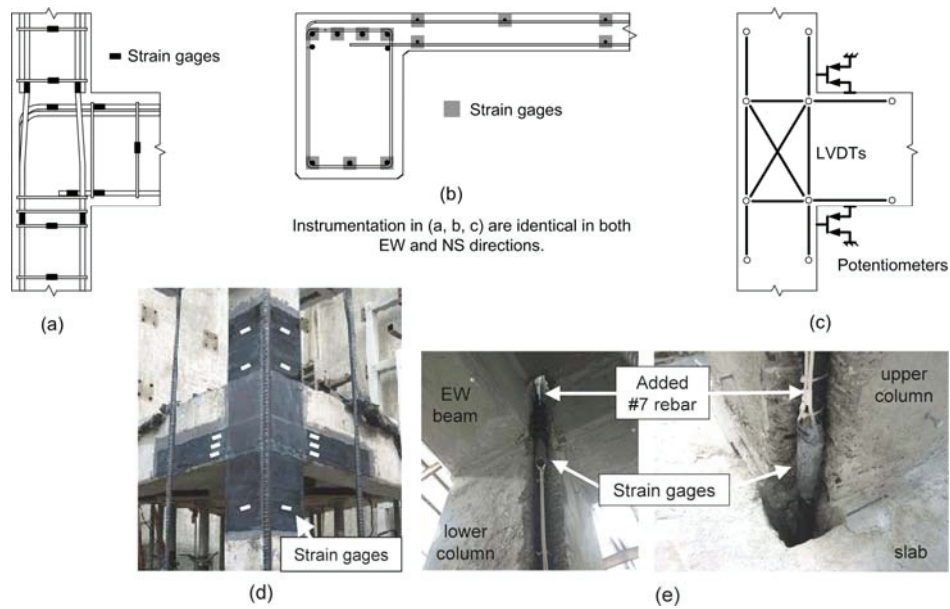


Figure 3 — Instrumentation.

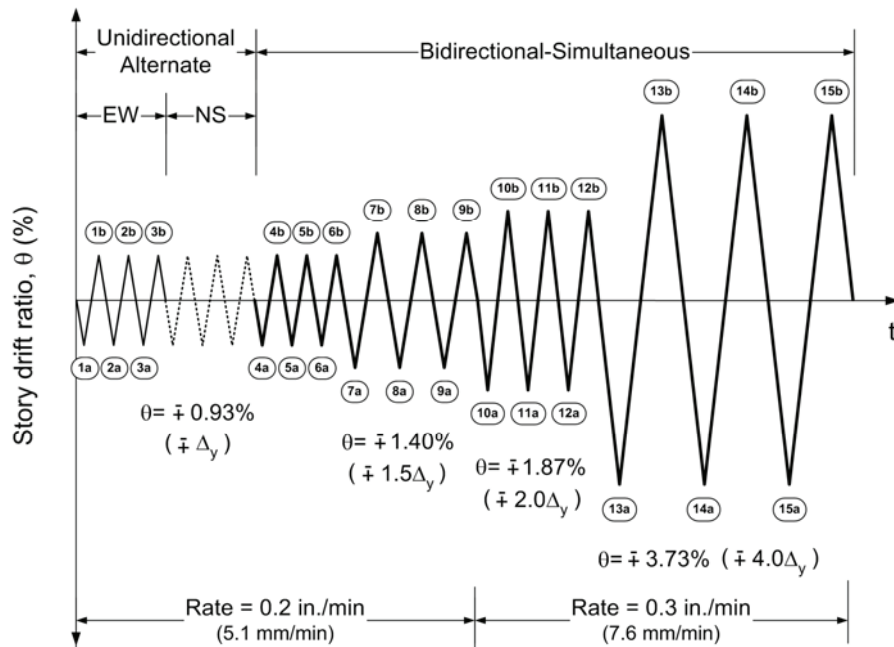


Figure 4 — Applied displacement history. Negative drift (downward beam displacement) causes tension at the top of the beams. Cycle 1 has negative peak 1a and positive peak 1b.

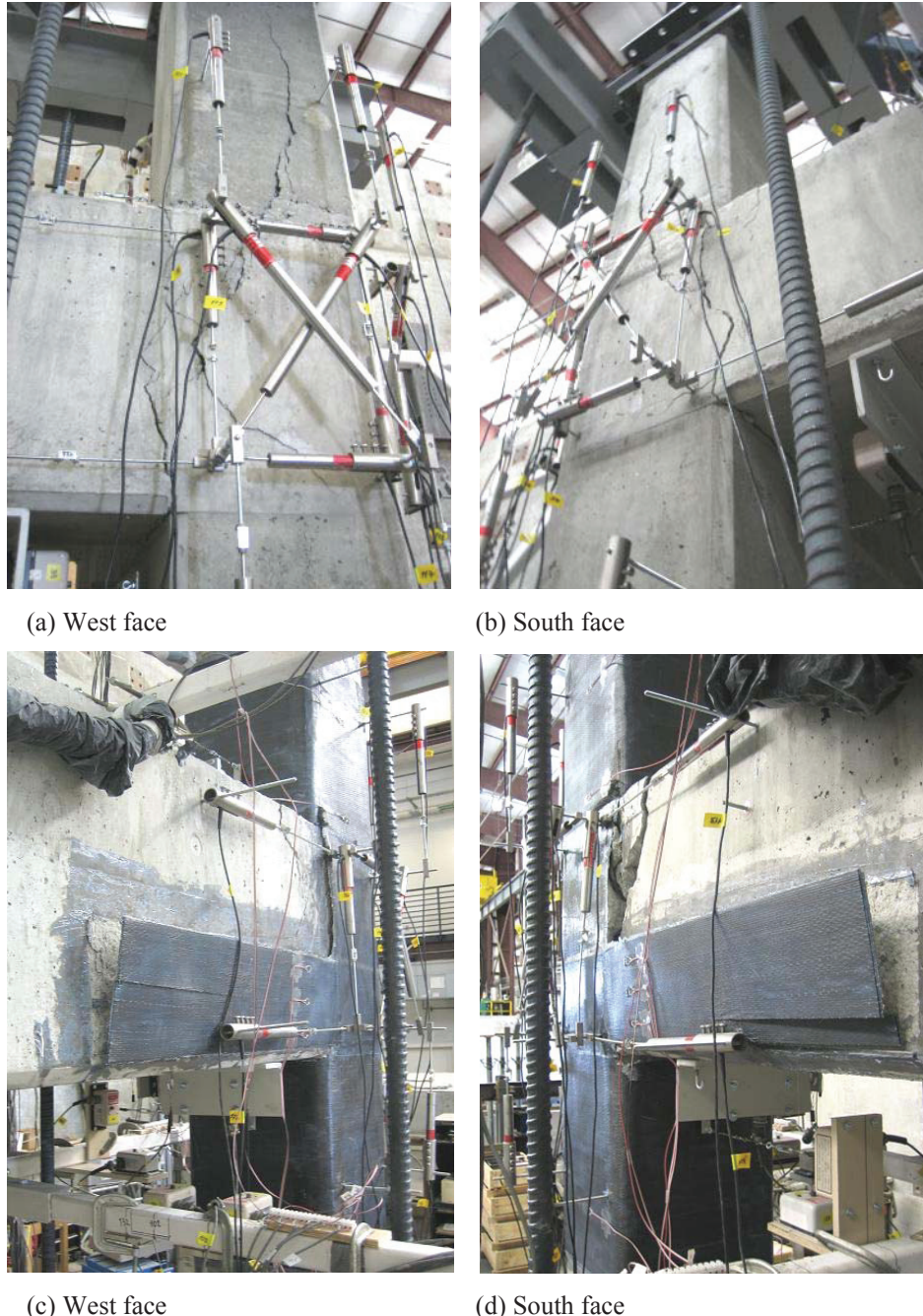
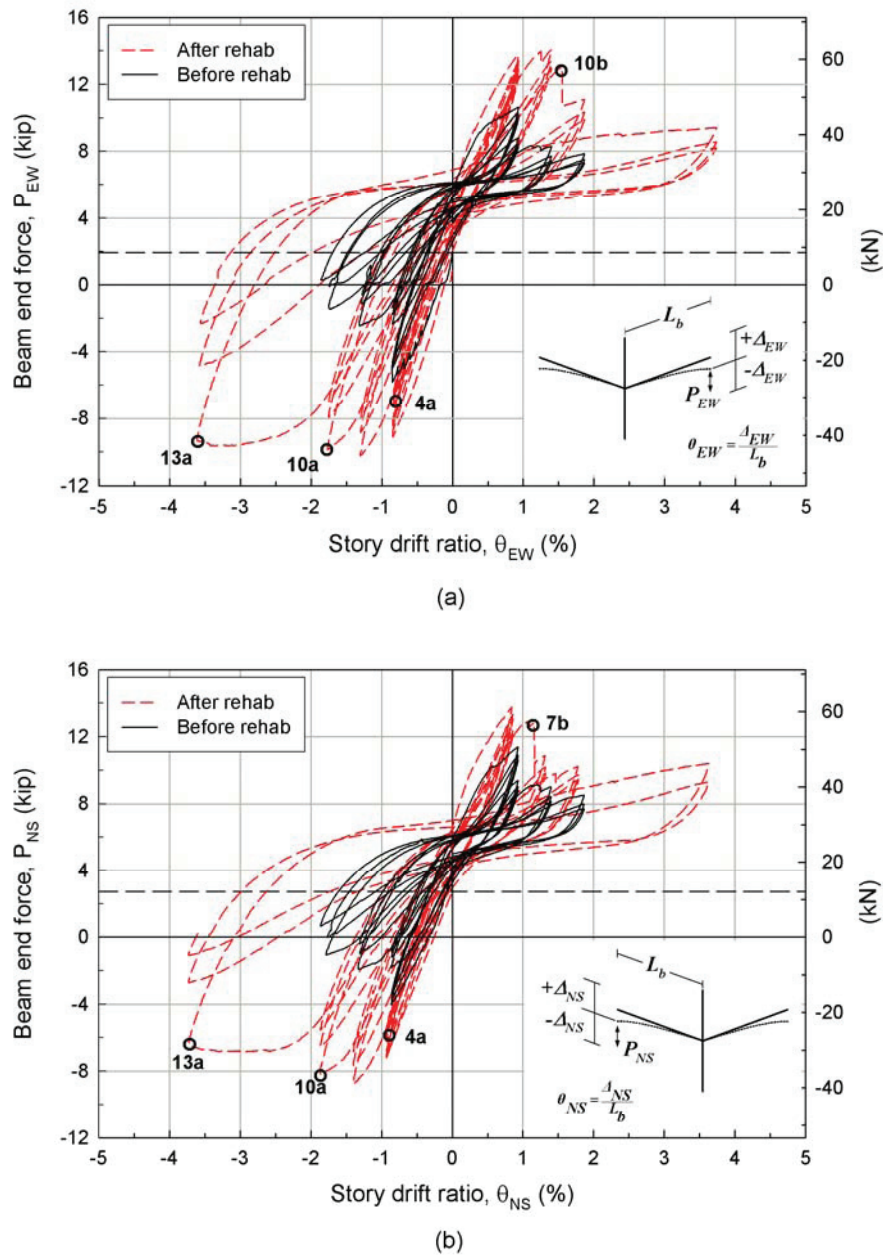


Figure 5 — Damage at the end of test: (a, b) before rehabilitation at cycle point 12a, and (c, d) after rehabilitation at cycle point 15a.



(4a) First yield in beams, (7b) Debonding of FRP strips on NS beam,  
 (10a) Extensive yielding in beams and first yield in column,  
 (10b) Debonding of FRP strips on EW beam, (13a) Joint failure

Figure 6 — Force-drift hysteresis loops: (a) EW, and (b) NS.

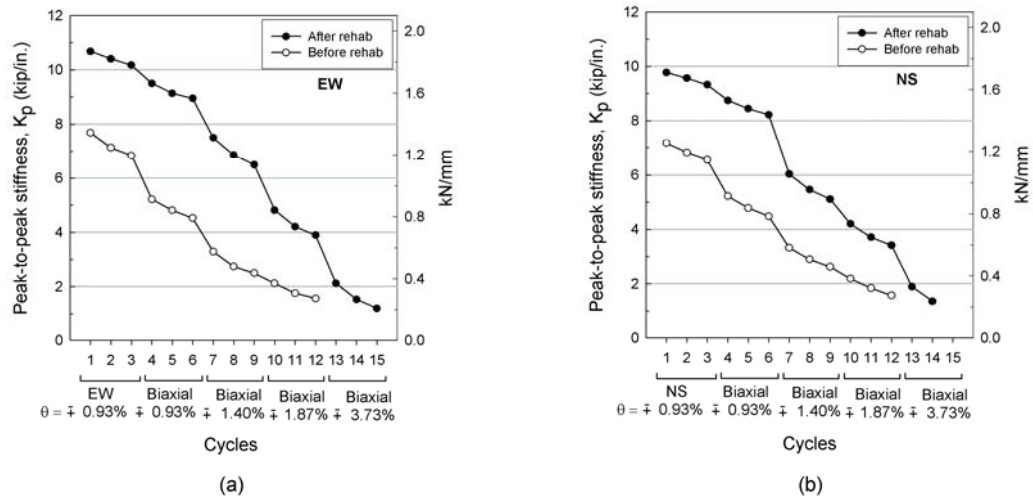


Figure 7 — Stiffness degradation: (a) EW, and (b) NS.

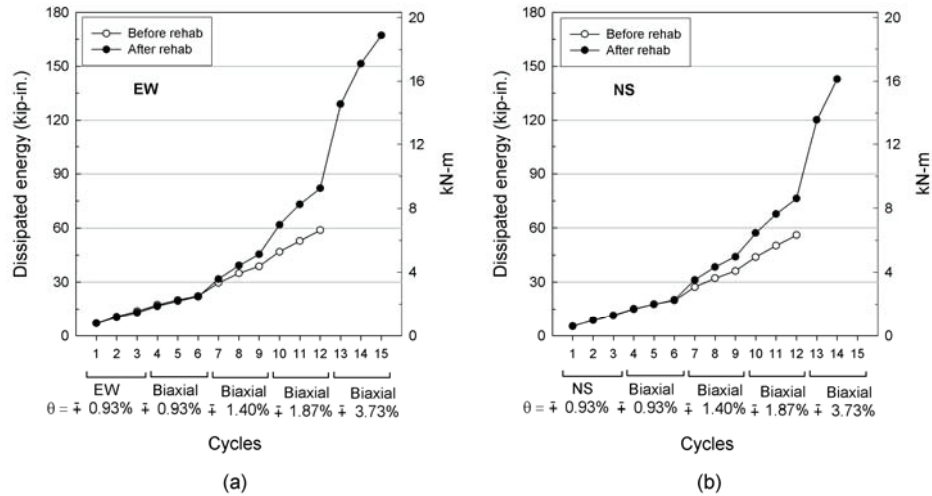


Figure 8 — Cumulative dissipated energy: (a) EW, and (b) NS.

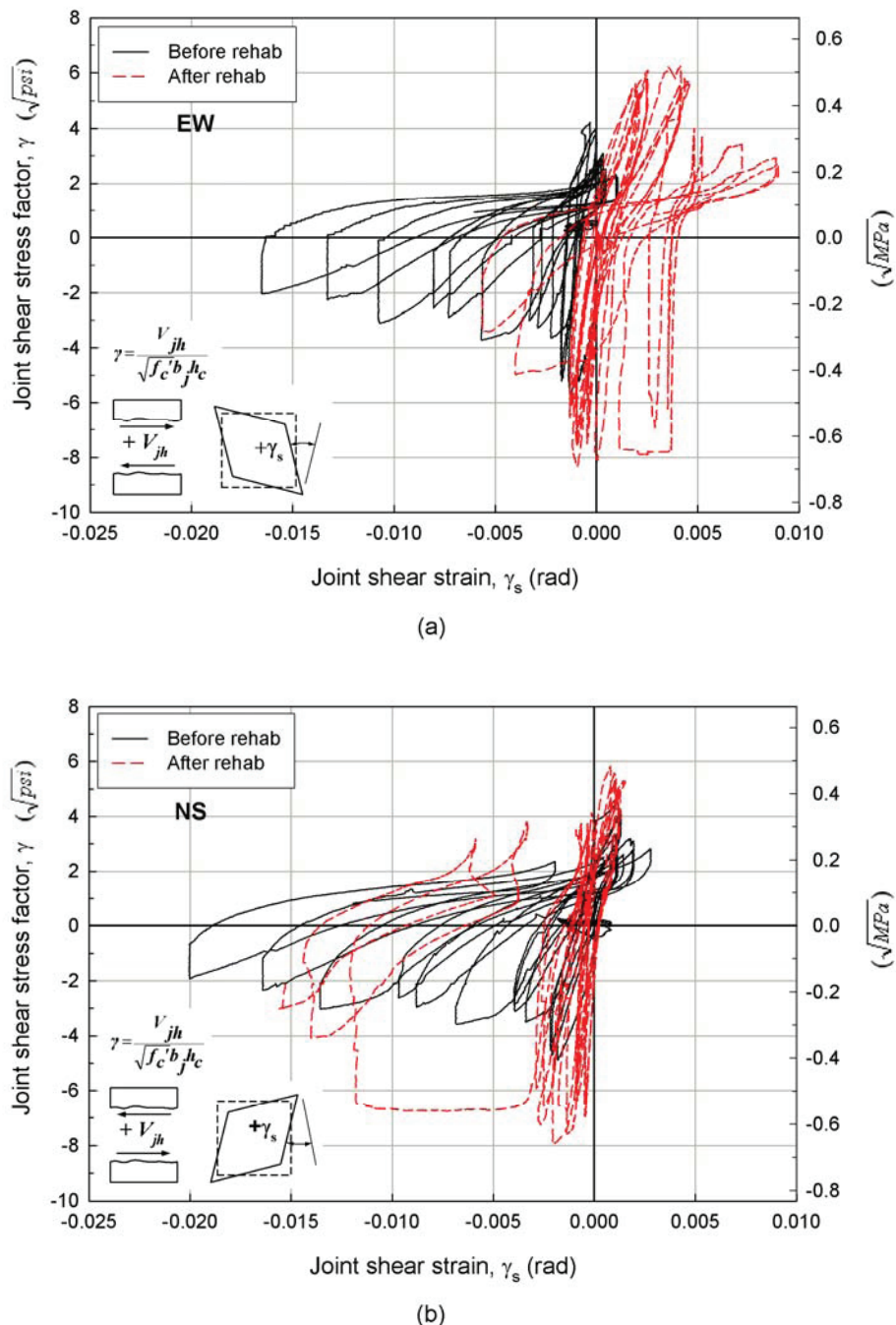


Figure 9 — Joint shear stress-strain hysteresis loops: (a) EW, and (b) NS.

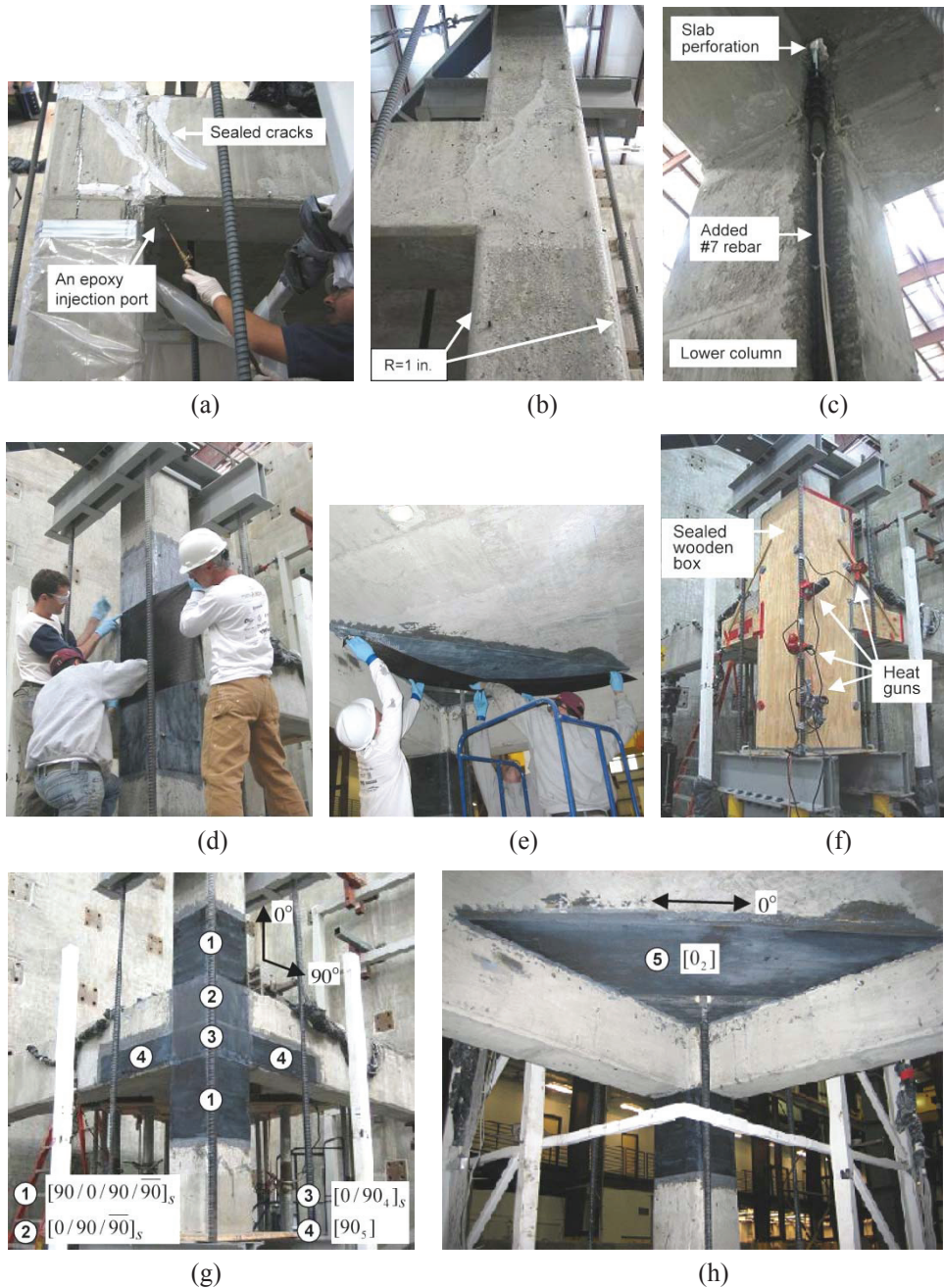


Figure 10 — Rehabilitation process: (a, b) epoxy injection and surface preparation, (c) addition of a #7 reinforcing bar, column inside corner, (d, e) CFRP application on column and bottom of slab, (f) heat-curing of CFRP, and (g, h) finished look.